

NASH: Neural Architecture and Accelerator Search for Multiplication-Reduced Hybrid Models

Yang Xu, Huihong Shi, and Zhongfeng Wang, *Fellow, IEEE*

Abstract—The significant computational cost of multiplications hinders the deployment of deep neural networks (DNNs) on edge devices. While multiplication-free models offer enhanced hardware efficiency, they typically sacrifice accuracy. As a solution, multiplication-reduced hybrid models have emerged to combine the benefits of both approaches. Particularly, prior works, i.e., NASA and NASA-F, leverage Neural Architecture Search (NAS) to construct such hybrid models, enhancing hardware efficiency while maintaining accuracy. However, they either entail costly retraining or encounter gradient conflicts, limiting both search efficiency and accuracy. Additionally, they overlook the acceleration opportunity introduced by accelerator search, yielding sub-optimal hardware performance. To overcome these limitations, we propose NASH, a Neural architecture and Accelerator Search framework for multiplication-reduced Hybrid models. Specifically, as for NAS, we propose a tailored zero-shot metric to pre-identify promising hybrid models before training, enhancing search efficiency while alleviating gradient conflicts. Regarding accelerator search, we innovatively introduce coarse-to-fine search to streamline search process. Furthermore, we seamlessly integrate these two levels of searches to unveil NASH, obtaining optimal model and accelerator pairing. Experiments validate our effectiveness, e.g., when compared with the state-of-the-art multiplication-based system, we can achieve $\uparrow 2.14\times$ throughput and $\uparrow 2.01\times$ FPS with $\uparrow 0.25\%$ accuracy on CIFAR-100, and $\uparrow 1.40\times$ throughput and $\uparrow 1.19\times$ FPS with $\uparrow 0.56\%$ accuracy on Tiny-ImageNet. Codes are available at <https://github.com/xuyang527/NASH>.

Index Terms—Multiplication-reduced hybrid model, zero-shot search, hardware accelerator, neural architecture and accelerator co-search, algorithm and hardware co-optimization.

I. INTRODUCTION

Despite the remarkable success of deep neural networks (DNNs) in various computer vision tasks [1], [2], [3], the involved intensive multiplications yield significant hardware costs, thus hindering DNNs' deployment on resource-constrained edge devices. To enhance hardware efficiency, prior works [4], [5], [6], [7], [8] have developed multiplication-free models that substitute multiplications with hardware-friendly operations, such as bitwise shifts and additions. For example, DeepShift [7] substitutes multiplications with bitwise shifts, thereby building models exclusively with shift layers. Besides, AdderNet [4] trades multiplications with additions,

This work was supported by the National Key R&D Program of China under Grant 2022YFB4400604.

Yang Xu and Huihong Shi contributed equally to this work, and are with the School of Electronic Science and Engineering, Nanjing University, Nanjing, China (e-mail: {xyang, shihh}@smail.nju.edu.cn).

Zhongfeng Wang is with the School of Electronic Science and Engineering, Nanjing University, and the School of Integrated Circuits, Sun Yat-sen University (email: zfwang@nju.edu.cn).

Correspondence should be addressed to Zhongfeng Wang.

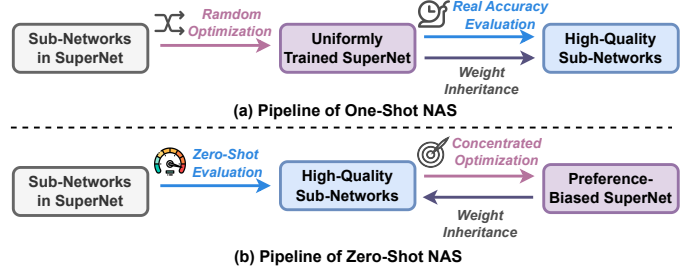


Fig. 1. Pipelines of (a) one-shot supernet-based NAS [11], [12] and (b) zero-shot NAS framework combined with preference-biased supernet training [13].

thus constructing models with solely adder layers. Furthermore, ShiftAddNet [8] integrates both shift and adder layers, developing models with merely hardware-friendly bitwise shifts and additions. Despite their notable hardware efficiency, multiplication-free models are generally inferior to their multiplication-based counterparts in accuracy [9], [10]. Thus, motivated by the high accuracy of multiplication-based models and the promising hardware efficiency of multiplication-free models, there is an urgent demand for multiplication-reduced hybrid models to marry the benefits of both multiplications and hardware-friendly operations.

To achieve this goal, prior works leverage Neural Architecture Search (NAS) to automatically design such multiplication-reduced hybrid models [9], [10], [14]. Specifically, NASA [14] proposes a dedicated differentiable NAS (DNAS) engine to automatically construct hybrid models in a differentiable manner, which yet requires an expensive retraining process for searched models. Subsequently, NASA-F [10] develops a tailored one-shot NAS method to fully optimize all sub-networks within the pre-defined multiplication-reduced hybrid supernet, thus achieving high accuracy without retraining/finetuning. Despite its effectiveness, one-shot NAS still suffers from several drawbacks. Specifically, as shown in Fig. 1 (a), (i) one-shot NAS typically involves the random sampling of sub-networks with diverse qualities during the supernet training stage, thus yielding gradient conflicts and hindering the achievable accuracy; Additionally, (ii) the accuracy evaluation through model inference is time-consuming, thereby decelerating the subsequent architecture search process. To solve these limitations, zero-shot metrics have been applied to predict promising networks before model optimization [15], [16], [17], [18], [19], [20]. For example, the recent work PreNAS [13] advocates using SNIP [15] to pre-identify potentially high-quality sub-networks before supernet training. By doing this, as illustrated in Fig. 1 (b), (i) assessment using zero-shot metrics has been

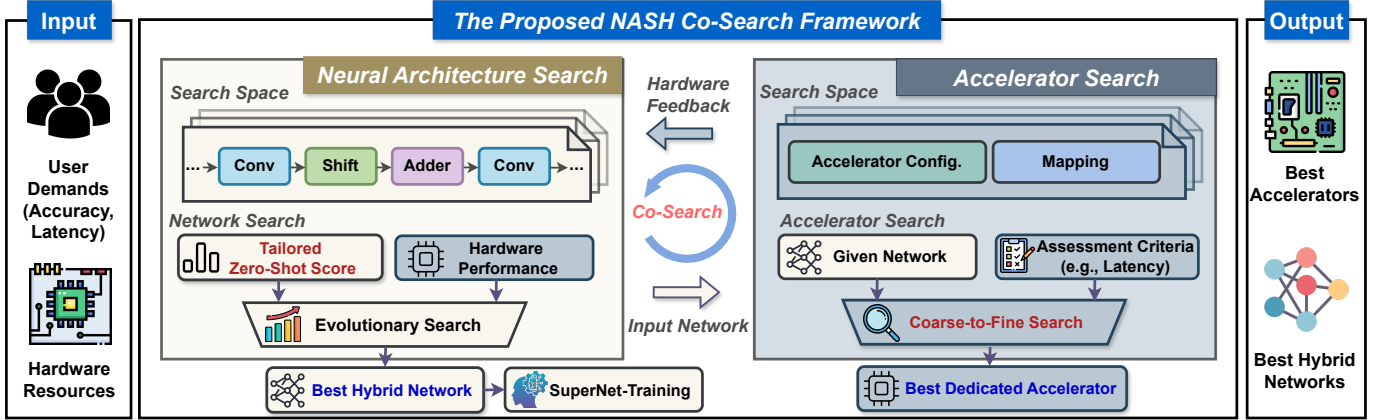


Fig. 2. The overview of our NASH framework, where we integrate both the neural architecture search (NAS) and coarse-to-fine accelerator search to directly obtain optimal pairing of models and accelerators. Specifically, the NAS consists of a tailored zero-shot metric to pre-identify promising multiplication-reduce hybrid models before supernet training. Besides, the accelerator search involves a novel coarse-to-fine search strategy to expedite the accelerator search process.

proven to be much faster than accuracy measurement [13], thus search efficiency is significantly enhanced; Besides, (ii) during the subsequent supernet training phase, training resources can be concentrated on these selected sub-networks instead of randomly sampled ones, allowing for the alleviation of gradient conflicts. However, due to the different algorithmic properties between multiplication-based convolutions and multiplication-free operations [4], [14], existing zero-shot metrics developed for multiplication-based models [15], [18], [19], [21] are not directly applicable to our desired multiplication-reduced models, calling for the exploration of tailored ones.

In parallel, various works [9], [10], [22] have developed dedicated accelerators to improve the hardware efficiency of DNNs from the hardware perspective. However, considering the intricate design space of accelerators, including the accelerator configuration (e.g., PE number and buffer size) and mapping method (also dubbed dataflow), it is non-trivial to handcraft an optimal dedicated accelerator, calling for automatic tools [23], [24], [25], [26], [27]. Specifically, NAAS [23] utilizes an evolutionary algorithm to search for the optimal accelerator configuration and mapping method. Then, it seamlessly integrates the accelerator search process with neural architecture search, thereby directly yielding the optimal pairing of model and accelerator. Inspired by its success, it is highly desired to leverage accelerator search to automatically build the accelerator dedicated to our desired multiplication-reduced hybrid model for boosting hardware efficiency. However, due to the distinct algorithmic properties exhibited by heterogeneous layers within the hybrid model, including convolution layers, shift layers, and adder layers, there arises a necessity to construct separate computing engines for each type of layer, aiming to enable independent processing [10], [14]. This inherently expands the search space and inevitably amplifies the search complexity of our dedicated accelerator [14], thus necessitating fast search strategies.

To this end, in pursuit of advancing the search efficiency, model accuracy, and hardware efficiency for multiplication-reduced hybrid models, we develop a neural architecture and accelerator co-search framework tailored to such hybrid

models, and make the following contributions:

- We propose **NASH** (see Fig. 2), a Neural architecture and Accelerator co-Search framework dedicated to multiplication-reduced Hybrid models. To the best of our knowledge, this is the first model-accelerator co-search framework for such hybrid models.
- On Neural Architecture Search (NAS) level, we develop a **tailored zero-shot metric** to pre-identify promising multiplication-reduced hybrid architectures before training, thus enhancing search efficiency as well as alleviating gradient conflicts during the subsequent supernet optimization to enhance accuracy.
- On the accelerator search level, considering the enormous search space of the accelerator dedicated to our hybrid models, we innovatively propose a **coarse-to-fine search strategy** to significantly expedite the accelerator search process. Besides, this accelerator search can be further integrated with the above NAS process to obtain NASH, aiming to directly obtain optimal pairing of multiplication-reduced models and dedicated accelerators.
- Extensive experimental results consistently validate our superiority. Particularly, we offer up to $\uparrow 0.56\%$ accuracy on Tiny-ImageNet over the prior multiplication-reduced work NASA-F, and $\uparrow 2.14\times$ throughput as well as $\uparrow 2.01\times$ FPS with $\uparrow 0.25\%$ accuracy against the state-of-the-art (SOTA) multiplication-based system on CIFAR100.

II. RELATED WORKS

A. Multiplication-Reduced DNNs

To alleviate the computational burden imposed by resource-dominant multiplications involved in DNNs, prior works have developed multiplication-free models with hardware-friendly alternatives, such as bitwise shifts [7] and additions [4], [5], [6], [28], thereby contributing to the progress in developing efficient models. For example, DeepShift [7] introduces shift layers that approximate multiplications using power-of-two equivalents, effectively substituting multiplications with bitwise shifts. AdderNets [4], [5], [6], [28] presents adder layers, which utilize the l_1 -normal distance to assess the similarity

between inputs and weights, thereby trading multiplications for additions. Furthermore, ShiftAddNet [8] integrates the aforementioned shift and adder layers, resulting in multiplication-free models primarily with both bitwise shifts and additions. However, despite the promising hardware efficiency of these multiplication-free DNNs, they generally suffer from lower accuracy compared to their multiplication-based counterparts [8], [10], [14], [28]. To this end, multiplication-reduced models [8], [9], [10], [14], [29], [30] are highly desired to marry the benefits of both multiplication-based and multiplication-free models, aiming to enhance hardware efficiency while maintaining accuracy. For instance, NASA [14] and NASA-F [10] integrate multiplication-based convolutions as well as multiplication-free shift and adder layers to construct hybrid search space, on top of which, they leverage search algorithms to automatically build multiplication-reduced hybrid models.

B. Neural Architecture Search (NAS)

Neural Architecture Search (NAS) [10], [11], [12], [14], [31], [32], [33], which aims to search for the optimal network through enormous model architectures, has emerged as an effective approach to automatically design efficient models with saved human effort and expert knowledge. Among them, *one-shot supernet-based NAS* [10], [11], [12], [31], [32], [33] has achieved remarkable results and typically consists of two stages: supernet training and resource-constrained architecture search, as shown in Fig. 1 (a). Specifically, in the supernet training process, sub-networks are generally randomly sampled and optimized. Subsequently, the resource-constrained architecture search is applied to identify the optimal network from the well-trained search space through accuracy evaluation while adhering to a specific resource constraint. For instance, NASA-F [10] develops a tailored one-shot NAS engine for multiplication-reduced models, aiming to maintain accuracy while enhancing hardware efficiency.

Recently, some frontier works [13], [15], [16], [18], [34] have proposed zero-shot metrics, aiming to pre-identify potentially promising architectures without model training. Motivated by this, PreNAS [13] advocates swapping the order of supernet training and search process in the standard one-shot NAS. Specifically, as depicted in Fig. 1 (b), it employs a zero-shot metric (i.e., SNIP [15]) to predict promising sub-networks, then allocates training resources to optimize the selected ones instead of randomly sampled ones to facilitate supernet training. However, zero-shot metrics tailored for multiplication-reduced hybrid models are still under-explored.

C. Accelerator Search

Considering the enormous design space within a dedicated accelerator, including (i) the hardware configurations specifying the hardware resource consumption in terms of buffers and computational resources and (ii) the mapping method (also dubbed dataflow) that indicates how computations are scheduled onto the accelerator, it is non-trivial to manually craft an optimal accelerator, which demands substantial expertise and iterative trials [23], [25], [35]. To solve this limitation,

accelerator search methodologies [23], [25], [35] have been developed to automatically identify both the optimal hardware configuration and mapping method, thus enhancing hardware efficiency. Additionally, the accelerator exploration can be further incorporated with the neural architecture search to directly obtain optimal pairing of models and accelerators [23], [35]. For instance, NAAS [23] formulates the network and accelerator co-search as a multi-loop process and employs an evolutionary algorithm to facilitate this complex procedure. Despite the effectiveness of the above works, they are exclusively tailored to designing accelerators for homogeneous networks that are characterized by merely multiplication-based operations. In light of the heterogeneous layers in our desired multiplication-reduced hybrid models, which include both multiplication-based and multiplication-free layers, the search space within the accelerator dedicated to such hybrid models becomes more intricate [9], [14], calling for more effective search solutions.

III. THE NEURAL ARCHITECTURE SEARCH

In this section, we first introduce our hybrid search space that integrates both multiplication-based convolutions and multiplication-free operations; Then, Sec. III-B illustrates our zero-shot search strategy that is equipped with a tailored zero-shot metric to pre-identify promising sub-networks within our hybrid search space before network training; Finally, Sec. III-C details our preference-biased supernet training, which concentrates training resources on these selected sub-networks, aiming to alleviate gradient conflict and boost accuracy.

A. The Hybrid Search Space

Fundamental Operations. To effectively search for desired multiplication-reduced models, we unify multiplication-based *convolutions* and multiplication-free *shift* and *adder layers* to construct our hybrid search space following [10]. Next, we will illustrate shift and adder layers, respectively.

- **Shift layers.** To enhance hardware efficiency, as outlined in Eq. (1), DeepShift [7] advocates the utilization of shift layers, where the weights W_{Shift} are derived by quantizing the vanilla convolutional weights W_{Conv} to their power-of-two equivalents following Eq. (2). By doing this, the costly multiplications in convolutions can be effectively substituted by hardware-efficient bitwise shifts.

$$Y = \sum X^T * W_{\text{Shift}}, \quad (1)$$

$$W_{\text{Shift}} = \hat{s} * 2^{\hat{p}}, \quad \text{where} \quad (2)$$

$$\hat{s} = \text{sign}(W_{\text{Conv}}), \quad \hat{p} = \text{round}(\log_2 |W_{\text{Conv}}|).$$

- **Adder layers.** As an alternative, as formulated in Eq. (3), AdderNet [4] builds adder layers that employ the l_1 -norm distance to measure the relevance between activations X and weights W_{adder} , thus trading multiplications with efficient additions.

$$Y = \sum -|X - W_{\text{adder}}|. \quad (3)$$

TABLE I

CHOICES OF THE CHANNEL NUMBER C , EXPANSION RATIO E , KERNEL SIZE K , OPERATION TYPE T , AND THE BLOCK NUMBER N IN OUR HYBRID SEARCH SPACE. {C, S, A} DENOTE {CONVOLUTIONS, SHIFT LAYER, ADDER LAYER}. MBPOOL REPRESENTS THE EFFICIENT LAST STAGE [36]

Block	C	E	K	T	N
First Conv	{16, 24}	-	1	C	-
Stage 1	{16, 24}	{1}	{3, 5}	{C, S, A}	{1, 2}
Stage 2	{24, 32}	{4, 5, 6}	{3, 5}	{C, S, A}	{3, 4, 5}
Stage 3	{32, 40}	{4, 5, 6}	{3, 5}	{C, S, A}	{3, 4, 5, 6}
Stage 4	{64, 72}	{4, 5, 6}	{3, 5}	{C, S, A}	{3, 4, 5, 6}
Stage 5	{112, 120, 128}	{4, 5, 6}	{3, 5}	{C, S, A}	{3, 4, 5, 6, 7, 8}
Stage 6	{192, 200, 208, 216}	{6}	{3, 5}	{C, S, A}	{3, 4, 5, 6, 7, 8}
Stage 7	{216, 224}	{6}	{3, 5}	{C, S, A}	{1, 2}
MBPool	{1792, 1984}	-	1	C	-

Supernet. By incorporating the above fundamental operations, we follow [10] to build our hybrid supernet. Specifically, As listed in Table I, the supernet mainly consists of seven stages, and each stage is composed of several inverted residual bottleneck (IRB) blocks [37] that comprise two point-wise (PW) layers separated by one depth-wise (DW) layer. There are five searchable parameters in each stage to specify a sub-network from the supernet: the output channel number of blocks/layers C , the channel expanding ratio of IRBs E , the kernel size of DW layers inside IRBs K , the layer type T , and the number of IRBs within a stage N .

B. Zero-Shot Search

1) *The Tailored Zero-shot Metric:* To alleviate gradient conflict during supernet training and boost accuracy, zero-shot metrics are highly desired to pre-identify high-quality sub-networks within our pre-defined hybrid search space before network optimization.

The Observation and Challenge. Zero-shot metrics tailored for multiplication-based models [15], [18], [20], [21], [38] have been widely explored and achieved remarkable success. However, we have observed non-negligible performance degradation when directly applying them to our multiplication-reduced models. Specifically, as demonstrated in Table II, the Kendall Tau Coefficient [39], a widely-used similarity measurement metric, between existing popular zero-shot metrics [15], [18], [19], [20], [21], [38], [40] and model accuracy is obviously higher in multiplication-based models than in our multiplication-reduced hybrid models. This underscores the necessity for customized solutions for our hybrid models, which is yet under-explored.

Our Proposed Solution. Existing zero-shot metrics typically assess networks’ performance based solely on trainability or expressivity [17], [42], resulting in biased measurements. To enable more accurate assessments, inspired by TE-NAS [17], we assess both the expressivity and trainability of models by integrating distinct zero-shot metrics, where the pivotal challenge lies in identifying effective zero-shot metrics tailored for our multiplication-reduced models.

a) *Trainability:* Models with high trainability can be effectively optimized via gradient descent, thus demonstrating high accuracy. To distinguish a powerful zero-shot metric for evaluating the trainability of our multiplication-reduced models, we first intuitively explore the widely-adopted gradient-based methods, including SNIP [15], Jacob covariance [38],

TABLE II

THE KENDALL TAU COEFFICIENT BETWEEN ZERO-SHOT METRIC SCORES AND REAL MODEL ACCURACY. T AND E ARE THE ABBREVIATIONS FOR TRAINABILITY AND EXPRESSIVITY

Metrics	Multi-based	Multi-reduced	Class
SNIP [15]	0.40	-0.01	T
Jacobian Covariant [38]	0.43	0.06	T
Grad Norm [21]	0.36	-0.09	T
Synflow [19]	0.47	0.06	T
Grasp [18]	0.35	0.03	T
Fisher [20]	0.45	-0.05	T
NN-Degree [34]	0.43	0.32	T
Linear Region Number [40]	0.32	0.19	E
Zen-Score [16], [41]	0.40	0.33	E
Ours	-	0.47	T&E

Grad Norm [21], Synflow [19], Grasp [18], and Fisher [20]. However, as depicted in Table II, they all suffer from severe performance drops. To gain deeper insights into this degradation, we take the representative gradient-based metric SNIP [15] as an illustrative example. Specifically, SNIP assesses model trainability by measuring the importance of its parameters in both the forward and backward processes and can be defined as follows:

$$\text{SNIP} = \sum_{i=1}^N |\langle \theta_i, \nabla_{\theta_i} \mathcal{L} \rangle|, \quad (4)$$

where $\langle \cdot \rangle$ donates the inner product, N , θ_i and \mathcal{L} are the number of layers, the parameter vector of the i -th layer within the given network, and the loss value, respectively. Unfortunately, in our multiplication-reduced hybrid models that includes both multiplication-free shift and adder layers alongside multiplication-based convolutions, occasions are more complicated. For example, weights are discrete and gradients are biased in shift layers [7]. Moreover, the value magnitude of both weights and gradients in adder layers are significantly larger than those in convolutions [4]. Therefore, due to the distinct behaviors of heterogeneous layers concerning weights and gradients, existing gradient-based zero-shot metrics designed for homogeneous models are inherently inapplicable to our hybrid models, yielding performance degradation.

To overcome this issue, we redirect our attention to the connectivity-based methods [34], [43], [44], which evaluate trainability through the analysis of models’ connectivity patterns (e.g., the topology of concatenation-type skip connections [34]). Particularly, we select NN-Degree [34], which is the SOTA one and can be formulated as:

$$\text{NN-Degree} = \sum_{i=1}^B \left(\frac{\sum_{j=1}^{N_i} C_{i,j}^O}{N_i} + \frac{C_i^R}{\sum_{j=1}^{N_i} C_{i,j}^I} \right), \quad (5)$$

where B denotes the total block number in a given network and N_i is the layer number of the i -th block. $C_{i,j}^O$ and $C_{i,j}^I$ are the output and input channel number of the j -th layer in the i -th block, and C_i^R is the residual connection channel number of the i -th block. As verified in Table II and Fig. 3, while NN-Degree does not exhibit the best predictive performance on multiplication-based models, it outperforms other gradient-based methods on our hybrid models. Besides, it enables faster evaluation as no gradient computation is involved.

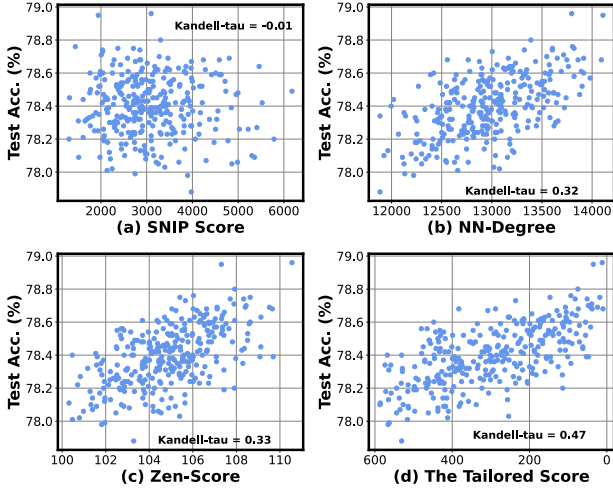


Fig. 3. Correlations between model accuracy and zero-shot metrics, including (a) SNIP, (b) NN-Degree, (c) Zen-Score, and (d) our tailored zero-shot metric, when measured on multiplication-reduced hybrid models.

b) Expressivity: Expressivity refers to the expressive capability of models. To identify the most effective zero-shot metric for the expressivity assessment of our hybrid models, we conducted experiments on two of the most well-known expressivity-based metrics: Linear Regions Number [40] and Zen-Score [16], [41]. Specifically, Linear Region Number assesses the expressivity of models by counting the number of unique linear regions within their input space [40]. Zen-Score measures models’ Gaussian complexity to evaluate their expressivity [16], [41] and can be formulated as follows:

$$\begin{aligned} \text{Zen-Score} = & \log \mathbb{E}_{\mathbf{x}, \epsilon} (\|f_e(\mathbf{x}) - f_e(\mathbf{x} + \alpha\epsilon)\|_F) \\ & + \sum_{k,i} \log \left(\sqrt{\frac{\sum_j \sigma_{ij}^k}{C_i^O}} \right), \end{aligned} \quad (6)$$

where \mathbf{x} is a sampled Gaussian random vector, ϵ is a small input perturbation, $\|\cdot\|_F$ is the Frobenius norm, α is a tunable hyper-parameter, C_i^O is the number of output channels of the i^{th} layer, and σ_{ij}^k is the variance of the k^{th} sample in an input batch data for the i^{th} layer’s j^{th} channel. As validated in Table II, Zen-Score shows superior estimation performance over Linear Region Number on both multiplication-based models and multiplication-reduced hybrid models. Additionally, it also exhibits better computational efficiency as counting the unique linear region number of large models involved in Linear Region Number has been proved to be very time-consuming [16]. Therefore, we select Zen-Score to assess the expressivity of our multiplication-reduced models.

c) Overall: To enable a more accurate assessment of our hybrid networks, we further integrate the aforementioned two selected zero-shot metrics. Specifically, given the significant difference in score *magnitudes* between these two metrics, as illustrated in Figs. 3 (b) and 3 (c), we add the relative *rankings* [17] instead of magnitudes of these two scores. Formally, given a group of networks \mathcal{N} , the score of our tailored zero-shot

metric for a specific network α is defined as follows:

$$\text{Score}(\alpha, \mathcal{N}) = \text{rank}(\text{Zen-Score}(\alpha), \text{Zen-Score}(\mathcal{N})) + \text{rank}(\text{NN-Degree}(\alpha), \text{NN-Degree}(\mathcal{N})), \quad (7)$$

where the first term computes the relative ranking of the Zen-Score of network α within the Zen-Scores of the network group \mathcal{N} . For instance, if α exhibits the highest Zen-Score among \mathcal{N} , the term yields a value of 0. Table II and Fig. 3 verify the effectiveness of our tailored zero-shot metric, which showcases the highest Kendall-Tau Correlation. It is noteworthy that our proposed metric also contributes to enhanced search efficiency, owing to the swift computational speed of both NN-Degree and Zen-Score. For example, the assessment of accuracy for an individual hybrid model derived from our supernet takes an average of 30 seconds, whereas the computation of our tailored zero-shot metric requires less than 2 seconds, which is over $15\times$ faster when tested on CIFAR100 and profiled on an NVIDIA GeForce RTX 2080Ti.

2) Neural Architecture Search: On top of the tailored zero-shot metric, we leverage the evolutionary algorithm (i.e., the genetic algorithm) [45] to expedite the pre-identification of promising sub-networks, aiming to alleviate gradient conflicts during the subsequent supernet training to boost accuracy. In detail, we first (i) randomly sample a population of sub-networks \mathcal{A} from our pre-defined hybrid supernet (see Sec. III-A and Table I); Then, (ii) we expand the population \mathcal{A} by crossover and mutation; Subsequently, (iii) we update \mathcal{A} by ranking candidates based on the score of our tailored zero-shot metric following Eq. (7) and retaining only the top-k ones $\tilde{\mathcal{A}}$, subject to given hardware constraints. Note that to enable fast and accurate estimations, we follow [10], [14] to build a cycle-accurate chip simulator on top of our dedicated accelerator (which will be introduced in Sec. IV) to measure hardware performance. Finally, steps (ii) to (iv) are iterated until the pre-determined iteration number is reached. The algorithm pipeline is outlined in Alg. 1 and will be detailed in Sec. IV-C.

C. Preference-Biased Supernet Training

After identifying promising hybrid sub-networks through our zero-shot search, training resources can be concentrated on these selected sub-networks via preference-biased supernet training, aiming to boost accuracy. To facilitate this process, we leverage the SOTA supernet training strategy in [10], [12], which includes a sandwich-rule-guided architecture sampling [11] and an α -divergence-based knowledge distillation [12]. Precisely, the training process can be defined as:

$$\min_{\theta} \mathbb{E}_{\alpha_r \sim \tilde{\mathcal{A}}} \{ \mathcal{L}_{\text{CE}}(\theta, \alpha_b) + \gamma [\mathcal{L}_{\text{KD}}(\theta, \alpha_s) + \sum_{i=1}^M \mathcal{L}_{\text{KD}}(\theta, \alpha_r^i)] \}, \quad (8)$$

where θ is the supernet weights, \mathcal{L}_{CE} denote the cross entropy loss, and γ is the loss coefficient. Besides, the sandwich rule is applied to simultaneously optimize the smallest sub-network α_s , the biggest sub-network α_b , and M random networks α_r from our pre-defined sub-networks pool $\tilde{\mathcal{A}}$, thus pushing forward both the performance lower bound (α_s) and upper bound (α_b) of $\tilde{\mathcal{A}}$. Additionally, \mathcal{L}_{KD} represent the α -divergence-based

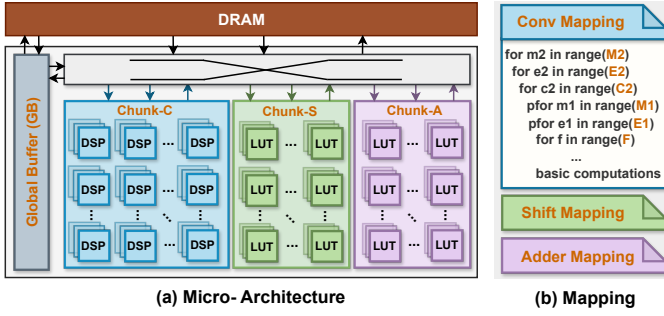


Fig. 4. (a) depicts the accelerator micro-architecture, which leverages distinct hardware resources on FPGAs to develop tailored chunks, dubbed Chunk-C, Chunk-S, and Chunk-A, to support convolutions, shift, and adder layers within searched hybrid models, respectively. (b) shows mapping methods (i.e., dataflows) for chunks using the widely adopted for-loop description [46]. Notably, components labeled in orange denote the searchable elements within our accelerator search space.

knowledge distillation, which leverages the soft logits from α_b to optimize α_r and α_s through α -divergence, aiming to alleviate the issue of under-estimation and over-estimation of vanilla knowledge distillation.

IV. THE ACCELERATOR SEARCH

In this section, we first introduce the micro-architecture and search space of our dedicated accelerator; Then we illustrate the proposed coarse-to-fine accelerator search strategy in Sec. IV-B, which divides the original vast accelerator search space into several smaller ones to enhance accelerator search efficiency; Finally, Sec. IV-C integrates the accelerator search with the previously introduced neural architecture search to unveil the comprehensive NASH framework.

A. Micro-Architecture and Search Space

Micro-architecture. To support our multiplication-reduced hybrid models, our dedicated accelerator advocates a chunk-based design, which incorporates several tailored chunks to independently process heterogeneous layers in multiplication-reduced hybrid models following [10], [14]. As illustrated in Fig. 4 (a), our accelerator mainly comprises an off-chip DRAM, an on-chip Global Buffer (GB), and three distinct chunks (i.e., sub-processors), dubbed Chunk-C, Chunk-S, and Chunk-A. Particularly, to enhance hardware utilization and overall throughput, we follow NASA-F [10] to employ diverse computing resources available on FPGAs to build customized processing elements (PEs) within each chunk. For instance, PEs in Chunk-C are built by Digital Signal Processors (DSPs), aiming to effectively support multiplications in convolutions. In contrast, PEs in Chunk-S/Chunk-A are developed via Look-Up Tables (LUTs) to efficiently handle bit-wise shifts/additions in shift/adder layers.

Search Space. To enable accelerator search, the (i) *hardware configuration*, including the PE number of each chunk and buffer size of GB, as well as (ii) *the mapping method* (i.e., dataflow), are searchable in our accelerator. Specifically, as for the search space of dataflow (see Fig. 4 (b)), we leverage the widely adopted nested for-loop description [46],

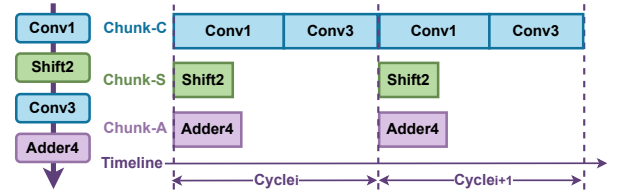


Fig. 5. Illustrating the processing timeline of our chunk-based accelerator, where we use a hybrid model consisting of four layers (Conv1, Shift2, Conv3, and Adder4) as an example. Due to the limited DSP resources available on FPGAs, DSP-based Chunk-C emerges as the most latency-dominated chunk in our accelerator.

which is characterized by loop ordering factors and loop tiling size. Among them, (i) the former describes the scheduling of computations among the PE array and within each PE, thereby determining data reuse patterns. To enhance search efficiency while maintaining generality, we search from four representative loop orders, including weight stationary (ws), output stationary (os), input stationary (is), and row stationary (rs), for each chunk. Hence, there are a total of $4 \times 4 \times 4 = 64$ combination patterns of mapping methods for our chunk-based accelerator, wherein three dedicated chunks independently handle convolutions, shift layers, and adder layers. (ii) Regarding the loop tiling size, it dictates how data are stored within each memory hierarchy to align with the specified loop tiling factors. It can be derived from all feasible choices within the given resource budget and model size constraint.

B. Coarse-to-Fine Search Strategy

Motivation. As discussed above, due to the existence of multiple chunks in our dedicated accelerator, the accelerator search space is *exponentially* expanded. Specifically, the combination choices of PE numbers alongside those of mapping methods are exponentially increased with the number of chunks, making it non-trivial to identify the optimal solution from such an enormous search space, thus calling for effective search strategies.

Processing Timeline. To enhance the comprehension of our upcoming proposed solution, we first introduce the processing timeline of our chunk-based accelerator. Particularly, data consumed by each chunk are independent within each cycle and are derived from different input images to facilitate the concurrent processing of chunks in our accelerator [10], [14], [47]. Fig. 5 employs a hybrid model comprising four layers as an illustrative example. As we can see, chunks in our accelerator, i.e., Chunk-C, Chunk-S, and Chunk-A, sequentially process their assigned layers, i.e., convolution layers (Conv1 and Conv3), shift layers (Shift2), and adder layers (Adder4), respectively. The outputs generated by each cycle will serve as input for the next cycle. To elaborate, the output of Conv1 managed by Chunk-C in Cycle_i will become the input for Shift2, which is then computed by Chunk-S in the subsequent Cycle_{i+1}. A cycle concludes once all chunks complete processing. Therefore, the overall latency is dominated by the chunk that consumes the most time.

Observation and Our Proposed Solution. As introduced in Sec. IV-A, our accelerator incorporates three dedicated

chunks, which leverage distinct computing resources available on FPGAs to independently support heterogeneous layers in our multiplication-reduced hybrid models, aiming to enhance resource utilization. Specifically, *Chunk-C* leverages DSP slices to effectively process multiplications in convolutions, while *Chunk-S/Chunk-A* utilizes LUTs to efficiently handle bit-wise shifts/additions in shift/adder layers. However, DSP slices are generally more resource-constrained compared to LUTs on FPGAs. For instance, on the widely-used embedded FPGA, Kria KV260, the number of LUTs surpasses that of DSP slices by approximately $100\times$. This discrepancy establishes *Chunk-C* as the most resource-constrained component. Nevertheless, as described in the above paragraph, the overall latency of our chunk-based accelerator is predominantly dominated by the chunk with the longest processing time. Consequently, the limited availability of DSP resources on the FPGA designates *Chunk-C* as the latency-bottleneck chunk.

Motivated by this observation, we innovatively introduce a coarse-to-fine accelerator search strategy, aiming to slim the search space and facilitate effective search. Firstly, we focus on identifying the optimal hardware configuration (i.e., PE number) and mapping method for the latency-dominated *Chunk-C* in a coarse granularity. Subsequently, we refine other searchable parameters in a fine granularity. By doing this, the original vast search space can be effectively partitioned into several smaller ones, which can be then sequentially explored. Thus, the search space is significantly slimmed and the search process is considerably expedited. Next, we will elaborate on our proposed coarse and fine search phases in detail.

Coarse Search. As analyzed above, due to the limited DSP resources on FPGAs, *Chunk-C* is the most latency-dominated chunk in our accelerator. To alleviate this bottleneck and enhance overall throughput, we first solely identify the optimal PE number and dataflow (including loop ordering factors and loop tiling size) for *Chunk-C* via the coarse search phase. Specifically, (i) as for the PE number, rather than exhaustively exploring all potential choices, we opt to directly set it to the maximum available value. This decision is driven by the fact that the available DSP resources, and consequently the allowable PE number in *Chunk-C*, have a direct impact on overall latency. Thus, this tailored handcrafted setting can ensure optimal performance for *Chunk-C* while mitigating the associated search cost. (ii) Regarding the tiling order and tiling size, we systematically iterate through all possible choices to identify the optimal dataflow. It is noteworthy that while previous works [23], [24] have employed complex algorithms to expedite this iteration process, they fall short of guaranteeing optimal results. Fortunately, due to our proposed coarse-to-fine search strategy and the resultant relatively small search spaces, the straightforward iteration-based search proves not only fast but also ensures optimal performance, aligning well with our coarse search phase. (iii) For other parameters excluded from the coarse search, the GB size is configured to its maximum available value to ensure optimal performance for *Chunk-C*, while the exploration of *Chunk-S* and *Chunk-A* is temporarily deferred for subsequent refinement.

Fine Search. After selecting the optimal PE number and dataflow for *Chunk-C*, we proceed to refine other searchable

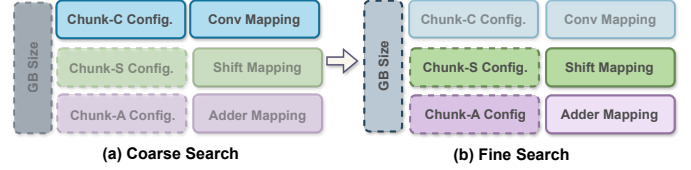


Fig. 6. Illustrating our coarse-to-fine accelerator search strategy. (a) In the coarse search, we first optimize the bottleneck *Chunk-C*. Subsequently, (b) in the fine search, we refine other searchable components, including *Chunk-S*, *Chunk-A*, and global buffer (GB).

parameters via the fine search phase. This involves searching for PE numbers and mapping methods for both *Chunk-S* and *Chunk-A*, along with determining the buffer size of GB. It can be easily observed that although the search space is significantly slimmed owing to our proposed coarse-to-fine search strategy, the fine search phase still encompasses a more extensive search space than the coarse search, challenging the feasibility of employing the iteration-based search method. To overcome this challenge and facilitate an effective search, we further streamline the search space associated with this fine search phase by capitalizing on the inherent hardware characteristics of our accelerator. Specifically, (i) as for PE numbers in *Chunk-S* and *Chunk-A*, considering *Chunk-C* dominates latency (see Fig. 5), excessive use of LUTs to construct redundant PEs for both *Chunk-S* and *Chunk-A* cannot expedite overall processing but rather incurs additional hardware resource consumption. Guided by this insight, we initialize PE numbers for *Chunk-S* $N_{\text{Chunk-S}}$ and *Chunk-A* $N_{\text{Chunk-A}}$ based on the predetermined PE number for *Chunk-C* $N_{\text{Chunk-C}}$ as well as the operation numbers of convolutions O_{Conv} , shift layers O_{Shift} , and adder layers O_{Adder} :

$$\frac{N_{\text{Chunk-C}}}{O_{\text{Conv}}} = \frac{N_{\text{Chunk-S}}}{O_{\text{Shift}}} = \frac{N_{\text{Chunk-A}}}{O_{\text{Adder}}}, \quad (9)$$

which means that the allocation of PEs to each chunk is determined by the operation number of its assigned layers, aiming to achieve a balanced execution time across chunks [10], [14]. Based upon this initialization, we only need to finetune $N_{\text{Chunk-A}}$ and $N_{\text{Chunk-S}}$ instead of iterating through all possible choices, thus significantly reducing search costs while preserving search accuracy. (ii) Thanks to the aforementioned simplification, we then allocate the saved search resources to thoroughly explore mapping methods for *Chunk-S* and *Chunk-A*, thus ensuring optimal dataflow. (iii) Finally, once PE numbers and mapping methods are established for all chunks, the buffer size of the GB is directly calculated as the minimum size required for computations [25] rather than exhaustive searching, increasingly facilitating the search process.

C. Neural Architecture and Accelerator Co-Search

By integrating the aforementioned accelerator search methodology into the previously introduced neural architecture search, we successfully derive our NASH neural architecture and accelerator search framework. Specifically, in the process of identifying promising multiplication-reduced sub-networks, we evaluate the algorithmic performance of models using our tailored zero-shot metric, as defined in Eq. (7). Furthermore,

Algorithm 1 NASH: Neural Architecture and Accelerator Co-Search for Multiplication-Reduced Models

Input: Hybrid model search space, accelerator search space, and hardware constraints

Output: Optimal network and dedicated accelerator pairing
// Evolutionary Search

Randomly sample a population of sub-networks \mathcal{A}

for $iter = 1$ **to** $max\ iteration$ **do**

 Expand the population \mathcal{A} by crossover and mutation

for *each network* α *in* \mathcal{A} **do**

// Hardware Evaluation

 Employ coarse-to-fine search following Sec. IV-B to obtain the **best accelerator** for network α

 Measure hardware performance for network α

// Algorithm Evaluation

 Compute $n = \text{NN-Degree}(\alpha)$ via Eq. (5)

 Compute $z = \text{Zen-Score}(\alpha)$ via Eq. (6)

end

 Compute zero-shot score s using z and n via Eq. (7)

 Update \mathcal{A} by selecting **networks with top- k** s under given hardware constraints

end

Do preference-biased supernet training via Eq. (8)

we estimate the optimal hardware performance of these models employing our proposed coarse-to-fine accelerator search strategy. Formally, we outline the computation pipeline of our NASH framework in Alg. 1, which seamlessly integrates both neural architecture search and accelerator search, aiming to directly identify optimal pairing of multiplication-reduced hybrid models and dedicated accelerators.

V. EXPERIMENTS

In this section, we first clarify our experimental setup, then compare our NASH framework with SOTA systems in Sec. V-B. Finally, we validate the effectiveness of our zero-shot architecture search and coarse-to-fine accelerator search enablers in Sec. V-C and Sec. V-D, respectively.

A. Experimental Setup

a) Datasets, Baselines, and Evaluation Metrics: To validate our NASH framework, which incorporates (i) a *zero-shot architecture search* to pre-identify promising multiplication-reduced models, thus alleviating gradient conflict during the subsequent preference-biased supernet training with boosted accuracy, and (ii) a *coarse-to-fine accelerator search* to partition and slim the enormous accelerator search space for accelerating the accelerator search process, we conduct experiments on *three datasets*, including CIFAR10, CIFAR100, and Tiny-Imagenet. We compare our NASH with *five baselines*, including SOTA *multiplication-based systems*: multiplication-based models searched by the SOTA multiplication-based (i) one-shot NAS work AlphaNet [12] and (ii) zero-shot search work PreNAS [13] and executed on the dedicated FPGA-based accelerator with SOTA DSP-implementations

[48] following [10]; SOTA *multiplication-free systems*, such as (iii) handcrafted multiplication-free models AdderNet [4] and (iv) DeepShift [7] executed on their dedicated FPGA accelerators with hardware-efficient LUT-implementations [10]; as well as the SOTA *multiplication-reduced system*, i.e., (v) multiplication-reduced models searched by the SOTA multiplication-reduced one-shot supernet-based NAS work NASA-F [10] and accelerated on its dedicated chunk-based accelerator. Moreover, we compare our NASH with other baselines in terms of *four evaluation metrics*: accuracy (top-1 accuracy by default), frame rate (Frame-Per-Second, FPS), overall throughput, and hardware utilization efficiency.

b) Search Setup: Our NASH integrates both neural architecture search and accelerator search. For the zero-shot *architecture search*, as introduced in Sec. III-B, to expedite the search process, we employ an evolutionary algorithm, where the population size is set to be 100, and the size and probability of mutation/crossover are set to be 50 and 0.2, respectively. We run the evolutionary search for 15 iterations, and only top-3 sub-architectures are retained during each iteration (i.e., $k = 3$ in our experiments).

For the *accelerator search*, we implement our accelerator on the widely-adopted Xilinx Kria KV260 embedded FPGA platform, which consists of 1248 DSP slices and 117k LUT resources, under a clock frequency of 200MHz. To provide fast and reliable estimations, we follow [10], [14] to build a cycle-accurate chip predictor/simulator upon our accelerator and validate it against the RTL implementation to ensure correctness. Additionally, we also follow [10], [14] to quantize both weights and activations into 8 bits, except weights in shift layers that are quantized into 4 bit.

c) Training Recipes: As introduced in Sec. III-C, optimization of identified sub-architectures is accomplished using the SOTA one-shot supernet-based training strategy [10], [12], which incorporates the sandwich rule-guided sampling method [11] and α -divergence-based knowledge distillation [12] to facilitate the supernet training. Specifically, (i) for CIFAR-10 and CIFAR-100, we optimize these sub-networks for 800 epochs, using the SGD optimizer with a momentum of 0.9. The initial learning rate (lr) is 0.3, which decays following a cosine scheduler. The batch size is set to 384. (ii) For the more challenging dataset Tiny-ImageNet, the training epoch is set to 250 epochs. Besides, the batch size and learning rate are adjusted to 128 and 0.1, respectively. The remaining settings are consistent with those employed in CIFAR10/CIFAR100.

B. NASH over SOTA Systems

a) Results and Analysis: As shown in Fig. 7, our NASH framework shows better trade-offs between accuracy and hardware efficiency over all SOTA baselines, demonstrating our effectiveness. Specifically, (i) by incorporating both hardware-efficient multiplication-free layers and powerful convolutions within our searched hybrid models, we significantly outperform SOTA *multiplication-based baselines* in hardware efficiency while maintaining comparable and even better accuracy. Particularly, when compared with the most competitive baseline, i.e., PreNAS [13] on the dedicated accelerator [10], we can offer

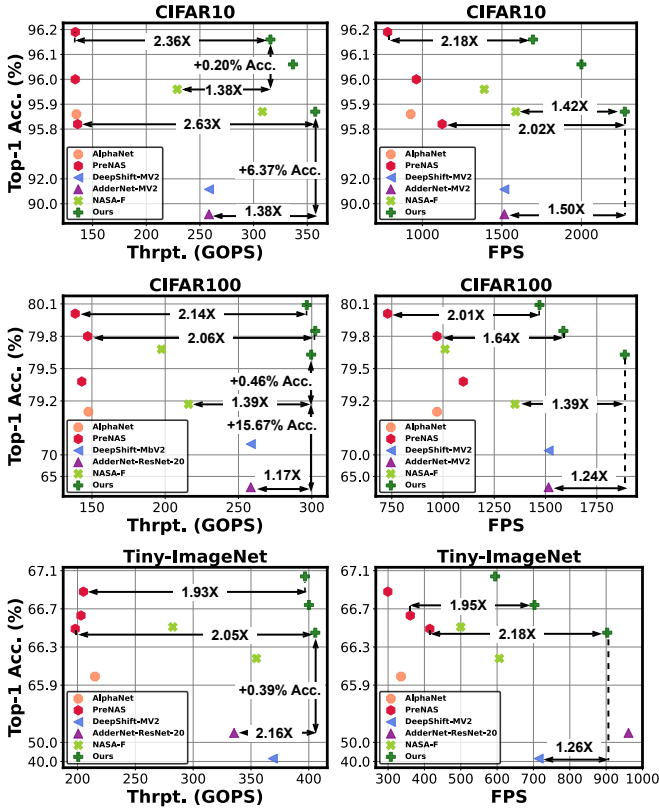


Fig. 7. Comparisons regarding throughput (Thrpt.) and FPS against accuracy when evaluated on CIFAR10, CIFAR100, and Tiny-ImageNet, respectively. MV2 donates the abbreviation of MobileNetV2 [37] by default.

$2.36\times\sim 2.63\times$, $2.06\times\sim 2.14\times$, and $1.93\times\sim 2.05\times$ throughput improvements alongside $2.02\times\sim 2.18\times$, $1.64\times\sim 2.01\times$, and $1.95\times\sim 2.18\times$ better FPS with $-0.07\%\sim 0.06\%$, $0.05\%\sim 0.25\%$, and $-0.04\%\sim 0.16\%$ higher accuracy, when tested on CIFAR10, CIFAR100, and Tiny-ImageNet, respectively.

(ii) Owing to the existence of convolutions within our searched hybrid models to enhance accuracy as well as the dedicated accelerator incorporated in our NASH framework to boost hardware efficiency, when compared with SOTA *multiplication-free systems*, we can offer much higher accuracy with comparable hardware efficiency. Specifically, we can offer up to $\uparrow 4.2\%$, $\uparrow 9.1\%$, and $\uparrow 23.3\%$ accuracy with $\uparrow 1.38\times$, $\uparrow 1.17\times$, and $\uparrow 1.10\times$ throughput as well as $\uparrow 1.50\times$, $\uparrow 1.24\times$, and $\downarrow 0.93\times$ FPS compared to the hand-crafted DeepShift-MobileNet-V2 [7] executed on its dedicated accelerator [10] and tested on CIFAR10, CIFAR100, and Tiny-ImageNet, respectively. Additionally, we can achieve $\uparrow 6.7\%$ and $\uparrow 16.6\%$ accuracy with $\uparrow 1.38\times$ and $\uparrow 1.17\times$ throughput alongside $\uparrow 1.50\times$ and $\uparrow 1.24\times$ FPS, when compared with AdderNet-MobileNet-V2 [4] on its dedicated accelerator [10] and evaluated on CIFAR-10 and CIFAR100, respectively.

(iii) As for comparisons with the SOTA *multiplication-reduced baseline* NASA-F [10], NASH also exhibits better accuracy and boosted hardware efficiency. This improved performance underscores the effectiveness of our tailored zero-shot metric in pre-identifying promising multiplication-reduced models, thus facilitating the subse-

quent supernet training. Additionally, it highlights the superiority of our coarse-to-fine accelerator search in the pursuit of optimal hardware performance. For instance, we can gain $\uparrow 1.16\times\sim\uparrow 1.38\times$, $\uparrow 1.40\times\sim\uparrow 1.50\times$, and $\uparrow 1.14\times\sim\uparrow 1.40\times$ throughput alongside $\uparrow 1.23\times\sim\uparrow 1.42\times$, $\uparrow 1.39\times\sim\uparrow 1.45\times$, and $\uparrow 1.19\times\sim\uparrow 1.49\times$ FPS with $0.19\%\sim 0.20\%$, $0.41\%\sim 0.46\%$, and $0.53\%\sim 0.56\%$ higher accuracy on CIFAR10, CIFAR100, and Tiny-ImageNet, respectively.

b) *Total Time Costs Comparisons*: We summarized our time costs regarding both supernet-training and search in Table III and compared them with other NAS baselines, including multiplication-based AlphaNet [12] and PreNAS [13], as well as multiplication-reduced NASA-F [10].

(i) For *supernet training*, compared to *multiplication-based baselines*, such as AlphaNet [12] and PreNAS [13], NASH takes a longer training time. This is mainly attributed to the slower training and inference speed of customized CUDA kernels for shift and adder layers compared to the PyTorch implementation for multiplications on GPUs [10], [30]. It is worth noting that this time cost overhead is essential for obtaining more hardware-friendly multiplication-reduced hybrid models. Particularly, despite integrating multiplication-free layers, we can achieve comparable accuracy against our most competitive baseline PreNAS [13]. Compared to the *multiplication-reduced baseline* NASA-F [10], we have similar training costs due to our similar training recipe. However, thanks to our proposed zero-shot metric utilized to pre-identify promising sub-networks, thus enabling a more advanced concentrated optimization during the subsequent supernet training, we can achieve higher accuracy, i.e., an average of $\uparrow 0.44\%$ accuracy on CIFAR100, further demonstrating our effectiveness.

(ii) For *architecture search*, due to the utilization of zero-shot metrics, both our NASH and PreNAS [13] can significantly reduce the search costs, when compared with methods that require real accuracy evaluation during network search (i.e., AlphaNet [12] and NASA-F [10]), verifying our search efficiency. Furthermore, to boost hardware efficiency, we integrate *hardware search* with network search, thus obtaining higher throughput. For example, we can achieve an average $\uparrow 45\%$ throughput against PreNAS on CIFAR100.

C. Evaluation of Our Zero-Shot Architecture Search

a) *Results and Analysis*: As presented in Tables IV and V, the models identified by our NASH framework demonstrate superior trade-offs between accuracy and computational cost. This substantiates our hypothesis that multiplication-reduced models are highly desired to marry the advantages of both convolutions and multiplication-free operators. Furthermore, this also underscores the effectiveness of our proposed zero-shot search in predicting promising multiplication-reduced models to boost accuracy. Specifically, (i) when compared with *multiplication-based models*, due to the incorporation of hardware-friendly multiplication-free operations, we can significantly save computational energy. Specifically, our energy reductions are $15.5\%\sim 24.7\%$, $3.8\%\sim 17.5\%$, and $17.3\%\sim 23.5\%$ compared to multiplication-based models searched by PreNAS [13] on CIFAR10, CIFAR100, and Tiny-ImageNet, respectively. Meanwhile, owing to the effectiveness

TABLE III

COMPARISONS OF TIME COSTS REGARDING BOTH SUPERNET-TRAINING AND SEARCH ON CIFAR100. 'THRPT.', 'ACC.', AND 'AVG.' ARE THE ABBREVIATIONS OF THROUGHPUT, ACCURACY, AND AVERAGE, RESPECTIVELY

Method	Supernet-Training		Search			Avg. Thrpt. (GOPS)	Avg. Acc. (%)
	Methodology	Time Cost	Network	Hardware	Total Time Cost		
AlphaNet [12]	Random Optimization	48h	6h	✗	6h	147.6	79.1
PreNAS [13]	Concentrated Optimization	48h	0.5h	✗	0.5h	142.9	79.73
NASA-F [10]	Random Optimization	84h	7h	✗	7h	206.7	79.42
Ours	Concentrated Optimization	84h	0.5h	5.5h	6h	299.5	79.86

TABLE IV

COMPARISONS BETWEEN OURS AND SOTA MULTIPLICATION-BASED/-FREE/-REDUCED BASELINES REGARDING OPERATION NUMBERS, COMPUTATIONAL ENERGY COSTS (COMP.), AND ACCURACY (ACC.), WHEN VALIDATED ON CIFAR10 AND CIFAR100, RESPECTIVELY

Models	Methods	CIFAR10					CIFAR100				
		Multi. (M)	Shift (M)	Add (M)	Comp. (mJ)	Acc. (%)	Multi. (M)	Shift (M)	Add (M)	Comp. (mJ)	Acc. (%)
Multi.-Based	AlphaNet [12]	72.86	0.00	72.86	0.437	95.86	76.02	0.00	76.02	0.456	79.10
	PreNAS-A [13]	85.46	0.00	85.46	0.513	96.19	94.82	0.00	94.82	0.569	80.01
	PreNAS-B [13]	69.85	0.00	69.85	0.419	96.00	75.90	0.00	75.90	0.455	79.80
	PreNAS-C [13]	60.37	0.00	60.37	0.362	95.82	64.92	0.00	64.92	0.390	79.38
Multi.-Free	DeepShift-MV2 [7]	6.60	79.20	85.80	0.154	91.90	6.70	79.20	85.80	0.154	71.00
	AdderNet-MV2 [4]	6.60	0.00	165.00	0.154	89.50	6.70	0.00	165.00	0.154	63.50
Multi.-Reduced	NASA-F-A [10]	50.87	28.53	85.42	0.351	95.96	72.48	15.68	107.34	0.471	79.68
	NASA-F-B [10]	46.78	43.88	103.60	0.353	95.87	53.26	18.82	87.70	0.358	79.17
	Ours-A	55.48	33.81	95.76	0.386	96.16	71.04	19.04	112.02	0.469	80.09
	Ours-B	47.97	33.81	88.24	0.341	96.06	65.97	18.64	105.78	0.438	79.85
	Ours-C	42.26	33.13	81.85	0.306	95.87	56.61	14.14	88.52	0.373	79.63

TABLE V

COMPARISONS OF OPERATION NUMBERS, COMPUTATIONAL ENERGY COSTS (COMP.), AND ACCURACY (ACC.) ON TINY-IMAGE NET

Models	Methods	Tiny-ImageNet				
		Multi. (M)	Shift (M)	Add (M)	Comp. (mJ)	Acc. (%)
Multi.-Based	AlphaNet [12]	320.43	0.00	320.43	1.923	65.99
	PreNAS-A [13]	342.44	0.00	342.44	2.055	66.88
	PreNAS-B [13]	281.17	0.00	281.17	1.687	66.63
	PreNAS-C [13]	238.64	0.00	238.64	1.432	66.49
Multi.-Free	DeepShift-MV2 [7]	19.77	215.03	234.80	0.428	43.70
	AdderNet-Res20 [4]	21.23	0.00	362.45	0.373	55.30
Multi.-Reduced	NASA-F-A [10]	212.96	52.28	299.61	1.378	66.51
	NASA-F-B [10]	167.59	98.40	319.25	1.186	66.18
	Ours-A	252.44	63.96	350.77	1.631	67.04
	Ours-B	216.02	54.49	298.75	1.395	66.74
	Ours-C	169.21	41.13	238.76	1.095	66.45

TABLE VI

THE RESOURCE CONSUMPTION OF DIFFERENT COMPUTATION TYPES WHEN IMPLEMENTED ON THE KRIA KV260 FPGA AND SYNTHESIZED UNDER THE FREQUENCY OF 200MHZ

Computation	Resource Consumption	
	LUT	DSP
Conv (Chunk-C)	37	0.5
Adder (Chunk-A)	29	0
Shift (Chunk-S)	34	0

of our zero-shot search strategy and preference-biased one-shot supernet-based training, we can maintain comparable and even better accuracy. Particularly, we can offer $-0.07\% \sim 0.25\%$ accuracy improvements over PreNAS [13].

(ii) As for comparisons with *multiplication-free models*, convolutions within our hybrid models enable us to largely outperform them in terms of accuracy. Particularly, we can

TABLE VII

COMPARISONS AMONG MODELS IDENTIFIED BY DIFFERENT ZERO-SHOT METRICS IN TERMS OF OPERATION NUMBERS, COMPUTATIONAL ENERGY COSTS (COMP.), AND ACCURACY (ACC.) ON CIFAR100

Methods	CIFAR100				
	Multi. (M)	Shift (M)	Add (M)	Comp. (mJ)	Acc. (%)
SNIP [15]	69.14	16.10	106.01	0.453	79.02
NN-Degree [34]	65.09	18.86	94.03	0.425	79.39
Zen-Score [16]	66.39	16.34	99.29	0.434	79.21
Ours-C	56.61	14.14	88.52	0.373	79.63

offer up to $4.2\% \sim 23.3\%$ and $6.7\% \sim 16.6\%$ higher accuracy over the handcrafted DeepShift-MobileNet-V2 [7] and AdderNet-MobileNet-V2 [4], respectively. It is worth noting that although our hybrid models consume more computational energy resulting from the incorporated convolutions, our dedicated chunk-based accelerator that supports the simultaneous processing of heterogeneous layers allows us to achieve comparable and even higher throughput and FPS (as demonstrated in Fig. 7), when compared with multiplication-free baselines.

(iii) Regarding comparisons with hybrid models searched by the SOTA *multiplication-reduced system* NASA-F [10], we demonstrate higher accuracy owing to the integration of proposed tailored zero-shot metric. Specifically, we can offer $0.19\% \sim 0.56\%$ higher accuracy. It is noteworthy that despite we gain comparable computational energy costs over NASA-F [10], we achieve higher throughput and FPS (as verified in Fig. 7). This is attributed to the effectiveness of our coarse-to-fine accelerator search strategy in enhancing hardware efficiency.

b) *Ablation Studies of Our Tailored Zero-Shot Metric:* To verify our tailored zero-shot metric, we compare it with

TABLE VIII

COMPARISONS REGARDING HARDWARE RESOURCE CONSUMPTION, THROUGHPUT (THRPT.), FPS, AND ACCURACY, WHEN EVALUATED ON CIFAR10

Method	Multiplication-Based				Multiplication-Free		Multiplication-Reduced				
	AlphaNet [12]	PreNAS-A [13]	PreNAS-B [13]	PreNAS-A-C [13]	DeepShift-MV2 [7]	AdderNet-MV2 [4]	NASA-F-A [10]	NASA-F-B [10]	Ours-A	Ours-B	Ours-C
Bitwidth	INT8	INT8	INT8	INT8	INT8	INT8	INT8	INT8	INT8	INT8	INT8
Strategy	DSP Implementations				LUT Implementations		DSP + LUT Implementations				
kLUT	41.3 (35.32%)	41.6 (35.54%)	41.3 (35.32%)	41.1 (35.11%)	46.2 (39.45%)	46.7 (39.88%)	63.9 (54.60%)	80.1 (68.48%)	61.7 (52.75%)	65.4 (55.94%)	66.4 (56.73%)
DSP	545 (43.7%)	545 (43.7%)	545 (43.7%)	545 (43.7%)	–	–	545 (43.7%)	545 (43.7%)	545 (43.7%)	545 (43.7%)	545 (43.7%)
BRAM	80 (27.7%)	80 (27.7%)	80 (27.7%)	80 (27.7%)	80 (27.7%)	80 (27.7%)	80 (27.7%)	80 (27.7%)	25.8 (8.9%)	19.4 (6.7%)	19.2 (6.7%)
Freq. (MHz)	200	200	200	200	200	200	200	200	200	200	200
Latency (ms)	1.08	1.28	1.04	0.89	0.66	0.66	0.72	0.63	0.59	0.50	0.44
Thrpt. (GOPS)	134.9	133.9	133.8	136.1	258.4	258.4	228.9	308.3	315.7	336.7	357.5
GOPS/kLUT	3.265	3.219	3.237	3.313	5.598	5.538	3.583	3.848	5.115	5.145	5.386
GOPS/DSP	0.248	0.246	0.245	0.250	–	–	0.420	0.566	0.579	0.618	0.656
FPS	925.9	783.2	957.6	1127.1	1515.2	1515.2	1388.9	1587.3	1706.2	1980.5	2273.6
HW Search	✗	✗	✗	✗	✗	✗	✗	✗	✓	✓	✓
Top-1 Acc. (%)	95.86	96.19	96.00	95.82	91.90	89.50	95.96	95.87	96.16	96.06	95.87

TABLE IX

COMPARISONS REGARDING HARDWARE RESOURCE CONSUMPTION, THROUGHPUT (THRPT.), FPS, AND ACCURACY, WHEN EVALUATED ON CIFAR100

Method	Multiplication-Based				Multiplication-Free		Multiplication-Reduced				
	AlphaNet [12]	PreNAS-A [13]	PreNAS-B [13]	PreNAS-A-C [13]	DeepShift-MV2 [7]	AdderNet-MV2 [4]	NASA-F-A [10]	NASA-F-B [10]	Ours-A	Ours-B	Ours-C
Bitwidth	INT8	INT8	INT8	INT8	INT8	INT8	INT8	INT8	INT8	INT8	INT8
Strategy	DSP Implementations				LUT Implementations		DSP + LUT Implementations				
kLUT	41.8 (35.71%)	42.4 (36.22%)	41.8 (35.71%)	41.4 (35.37%)	47.2 (40.31%)	48.2 (41.16%)	53.4 (45.63%)	58.8 (50.26%)	62.3 (53.21%)	59.5 (50.82%)	59.5 (50.82%)
DSP	545 (43.7%)	545 (43.7%)	545 (43.7%)	545 (43.7%)	–	–	545 (43.7%)	545 (43.7%)	545 (43.7%)	545 (43.7%)	545 (43.7%)
BRAM	80 (27.7%)	80 (27.7%)	80 (27.7%)	80 (27.7%)	80 (27.7%)	80 (27.7%)	80 (27.7%)	80 (27.7%)	39.0 (13.5%)	26.5 (9.2%)	19.2 (6.7%)
Freq. (MHz)	200	200	200	200	200	200	200	200	200	200	200
Latency (ms)	1.03	1.37	1.03	0.91	0.66	0.66	0.99	0.74	0.68	0.63	0.53
Thrpt. (GOPS)	147.6	138.6	147.1	143.1	258.4	258.4	197.5	215.9	296.6	302.4	299.6
GOPS/kLUT	3.533	3.271	3.520	3.459	5.479	5.366	3.699	3.672	4.764	5.086	5.038
GOPS/DSP	0.271	0.254	0.270	0.263	–	–	0.362	0.396	0.544	0.555	0.550
FPS	970.9	731.0	968.8	1102.4	1515.2	1515.2	1010.1	1351.4	1467.5	1588.4	1880.9
HW Search	✗	✗	✗	✗	✗	✗	✗	✗	✓	✓	✓
Top-1 Acc. (%)	79.1	80.01	79.80	79.38	71.00	63.50	79.68	79.17	80.09	79.85	79.63

TABLE X

COMPARISONS REGARDING HARDWARE RESOURCE CONSUMPTION, THROUGHPUT (THRPT.), FPS, AND ACCURACY ON TINY-IMAGENET

Method	Multiplication-Based				Multiplication-Free		Multiplication-Reduced				
	AlphaNet [12]	PreNAS-A [13]	PreNAS-B [13]	PreNAS-C [13]	AdderNet-ResNet-20 [4]	DeepShift-MV2 [7]	NASA-F-A [10]	NASA-F-B [10]	Ours-A	Ours-B	Ours-C
Bitwidth	INT8	INT8	INT8	INT8	INT8	INT8	INT8	INT8	INT8	INT8	INT8
Strategy	DSP Implementations				LUT Implementations		DSP + LUT Implementations				
kLUT	42.9 (36.65%)	43.1 (36.82%)	42.0 (35.88%)	41.7 (35.62%)	48.3 (41.28%)	60.9 (52.05%)	52.6 (44.97%)	67.7 (57.89%)	54.5 (46.57%)	55.2 (47.17%)	56.3 (48.16%)
DSP	545 (43.67%)	545 (43.67%)	545 (43.67%)	545 (43.67%)	–	–	545 (43.67%)	545 (43.67%)	545 (43.67%)	545 (43.67%)	545 (43.67%)
BRAM	80 (27.7%)	80 (27.7%)	80 (27.7%)	80 (27.7%)	80 (27.7%)	80 (27.7%)	80 (27.7%)	80 (27.7%)	52.5 (18.2%)	44.8 (15.5%)	73.0 (25.3%)
Freq.(MHz)	200	200	200	200	200	200	200	200	200	200	200
Latency (ms)	2.98	3.34	2.77	2.41	1.4	1.04	2	1.65	1.68	1.42	1.11
Thrpt. (GOPS)	215.1	205.1	203.0	198.0	335.4	368.9	282.4	354.7	396.7	400.1	405.6
GOPS/kLUT	5.015	4.760	4.836	4.751	6.945	6.058	5.368	5.237	7.280	7.249	7.197
GOPS/DSP	0.395	0.376	0.372	0.152	–	–	0.518	0.651	0.728	0.734	0.744
FPS	335.6	299.4	361.0	414.9	714.3	961.5	500.0	606.1	594.6	702.8	903.0
HW Search	✗	✗	✗	✗	✗	✗	✗	✗	✓	✓	✓
Top-1 Acc. (%)	65.99	66.88	66.63	66.49	55.3	43.7	66.51	66.18	67.04	66.74	66.45

three SOTA baselines, including SNIP [15], NN-Degree [34] and Zen-Score [16]. As shown in Table VII, (i) sub-network identified by our proposed metric achieves the highest accuracy with much fewer computational energy costs after the supernet training on CIFAR100, demonstrating our effectiveness in predicting promising multiplication-reduced hybrid models to alleviate gradient conflicts and boost accuracy. Specifically, we gain $\uparrow 0.61\%$, $\uparrow 0.24\%$, and $\uparrow 0.42\%$ accuracy with $\downarrow 0.82\times$, $\downarrow 0.88\times$, and $\downarrow 0.86\times$ computational energy costs compared to SNIP, NN-Degree, and Zen-Score, respectively. Besides, (ii) while Zen-Score and NN-Degree individually surpass the gradient-based SNIP by $\uparrow 0.37\%$ and $\uparrow 0.19\%$ accuracy with fewer computational costs, our tailored metric further enhances accuracy by combining both, which allows us to access both expressivity and trainability of models.

D. Evaluation of Coarse-to-Fine Accelerator Search

a) **Results and Analysis:** As illustrated in Tables VIII, IX and X, where the first, second, and third ranking performances are noted with corresponding colors, we achieve superior hardware efficiency (i.e., the overall throughput, hardware utilization efficiency w.r.t. both DSPs and LUTs, and FPS). This effectiveness highlights our chunk-based design, which utilizes heterogeneous computing resources available on FPGAs to construct customized chunks with enhanced hardware utilization and improved throughput. Besides, this also underscores the efficacy of our coarse-to-fine accelerator search strategy in fully unleashing hardware acceleration opportunities. Specifically, (i) when compared with *multiplication-based baselines*, due to the utilization of heterogeneous computing resources, which yields enhanced utilization efficiency

in DSPs and LUTs, our throughput and FPS are greatly improved. Particularly, we can achieve up to $\uparrow 1.63\times$, $\uparrow 1.46\times$, and $\uparrow 1.53\times$ DSP utilization efficiency alongside $\uparrow 2.63\times$, $\uparrow 2.14\times$, and $\uparrow 2.05\times$ LUT utilization efficiency on CIFAR10, CIFAR100, and Tiny-ImageNet, respectively.

(ii) In comparisons to *multiplication-free baselines*, which solely rely on LUTs to process additions or bitwise shifts, thus obtaining the highest LUT utilization efficiency, we can offer comparable and even better throughput and FPS with much higher accuracy. This is attributed to our chunk-based design that simultaneously processes heterogeneous layers within our hybrid models with distinct customized chunks.

More specifically, we have lower *GOPS/kLUT* on CIFAR10 and CIFAR100, and higher *GOPS/kLUT* on Tiny-ImageNet. The lower performance on CIFAR10 and CIFAR100 is mainly due to *higher LUT consumption* by the convolution-dedicated computing engine (Chunk-C) compared to the multiplication-free adder (Chunk-A) and shift layers (Chunk-S), as shown in Table VI. This higher LUT consumption in Chunk-C stems from three factors. 1) We follow NASA-F [10] to employ the SOTA DSP-packing strategy [48] to pack two 8-bit multiplications within one DSP, which enhances DSP utilization efficiency but yields additional LUT consumption. 2) Higher bit-width representations in convolutions require larger registers (e.g., 8-bit weights and 15-bit outputs in convolutions vs. 4-bit weights in shift layers and 9-bit outputs in adder layers), which leads to increased LUT consumption. (iii) Larger output bit-widths also necessitate bigger accumulators, further increasing LUT usage. Despite the higher LUT consumption in Chunk-C, our models searched on Tiny-ImageNet are significantly larger compared to handcraft multiplication-based models. The larger model sizes not only improve accuracy but also enhance hardware utilization, leading to improved *GOPS/kLUT* on this challenging dataset.

For *FPS*, compared to multiplication-free baselines, we achieve higher FPS on CIFAR10, comparable FPS on CIFAR100, and lower FPS on Tiny-ImageNet. This variation in performance is primarily influenced by *operation numbers*. Contrary to handcrafted multiplication-free models, which use the same architecture across all datasets and thus inevitably yield accuracy degradation on more challenging datasets, our NAS algorithm automatically searches for models of varying sizes tailored to each dataset to preserve accuracy, thereby resulting in different FPS outcomes.

Note that in situations where our hardware efficiency is lower compared to multiplication-free baselines, our superiority primarily lies in significantly *higher accuracy*, as outlined in Secs. V-B and V-C. Despite the promising hardware efficiency of multiplication-free baselines, with the integration of our dedicated accelerator, we can provide comparable or even superior hardware efficiency in certain scenarios, as discussed in the above paragraphs.

(iii) When compared with the SOTA *multiplication-reduced baseline* NASA-F [10], owing to our proposed coarse-to-fine accelerator search strategy, we can gain better hardware efficiency (i.e., higher FPS and throughput) with less hardware resource consumption (i.e., higher DSP and LUT utilization efficiency). For example, we can gain up to $\uparrow 1.44\times$, $\uparrow 1.39\times$,

TABLE XI
COMPARISONS OF SEARCH ACCURACY AND SEARCH EFFICIENCY AMONG VARIOUS SEARCH STRATEGIES WHEN TESTED ON CIFAR100. THE SEARCH TIME COST AND AVERAGE THROUGHPUT (AVG. THRPT.) OF THE SEARCHED ACCELERATOR ARE PROVIDED.

Coarse Search	Fine Search	Avg. Thrpt. (GOPS)	Time Cost
✗	✗	299.5	73 hours
✓	✗	254.0	2 hours
✗	✓	292.4	4 hours
✓	✓	299.5	5.5 hours

and $\uparrow 1.36\times$ DSP utilization efficiency as well as $\uparrow 1.47\times$, $\uparrow 1.39\times$, and $\uparrow 1.42\times$ LUT utilization efficiency, when tested on CIFAR10, CIFAR100, and Tiny-ImageNet, respectively.

b) Ablation Studies of Coarse-to-Fine Search Strategy:

To demonstrate the efficiency and accuracy of our coarse-to-fine search strategy, we compare it with three search strategies. As listed in Table XI: (i) Iteratively exploring the vanilla huge search space; (ii) Solely performing coarse search for Chunk-C and manually designing other components following NASA-F [10]; (iii) Manually designing Chunk-C following NASA-F [10] while performing fine search for other components. As verified in Table XI, when compared with (i), we can achieve comparable throughput with a much faster search speed, demonstrating our effectiveness. As for comparisons with (ii) and (iii), we can gain higher throughput with negligible time overheads, further highlighting our superiority in boosting hardware efficiency while enhancing search efficiency.

VI. CONCLUSION

This paper introduces, formulates, and validates NASH, a Neural architecture and Accelerator co-Search framework dedicated to multiplication-reduced Hybrid models. Specifically, regarding *neural architecture search*, we introduce a *tailored zero-shot metric* to pre-identify promising multiplication-reduced sub-architectures before supernet training, thus enhancing search efficiency while boosting accuracy. In terms of *accelerator search*, we innovatively propose a *coarse-to-fine accelerator search strategy* to expedite the accelerator search process and improve hardware efficiency. Furthermore, we integrate the neural architecture search with accelerator search to obtain NASH, aiming to directly obtain the optimal pairing of hybrid models and dedicated accelerators. Extensive experimental results validate our effectiveness. Particularly, we offer $\uparrow 0.56\%$ accuracy on Tiny-ImageNet compared to the prior multiplication-reduced work NASA-F, and up to $\uparrow 2.14\times$ throughput and $\uparrow 2.01\times$ FPS with $\uparrow 0.25\%$ accuracy over the state-of-the-art multiplication-based system on CIFAR100.

We will focus on two aspects in the future: (i) Improving the predictive accuracy of the tailored zero-shot metric to enhance accuracy. (ii) Expanding the dataflow search space beyond the typical four dataflows to enable a more comprehensive accelerator search.

REFERENCES

- [1] K. He, X. Zhang, S. Ren, and J. Sun, "Deep residual learning for image recognition," *2016 IEEE Conference on Computer Vision and Pattern Recognition (CVPR)*, pp. 770–778, 2016.

- [2] C. Szegedy *et al.*, “Going deeper with convolutions,” *2015 IEEE Conference on Computer Vision and Pattern Recognition (CVPR)*, pp. 1–9, 2015.
- [3] J. Redmon and A. Farhadi, “Yolo9000: Better, faster, stronger,” *2017 IEEE Conference on Computer Vision and Pattern Recognition (CVPR)*, pp. 6517–6525, 2017.
- [4] H. Chen *et al.*, “Addernet: Do we really need multiplications in deep learning?” *2020 IEEE/CVF Conference on Computer Vision and Pattern Recognition (CVPR)*, pp. 1465–1474, 2020.
- [5] Y. Xu *et al.*, “Kernel based progressive distillation for adder neural networks,” *ArXiv*, vol. abs/2009.13044, 2020.
- [6] H. Shu, J. Wang, H. Chen, L. Li, Y. Yang, and Y. Wang, “Adder attention for vision transformer,” in *Neural Information Processing Systems*, 2021.
- [7] M. Elhoushi, F. Shafiq, Y. Tian, J. Li, and Z. Chen, “Deepshift: Towards multiplication-less neural networks,” *ArXiv*, vol. abs/1905.13298, 2019.
- [8] H. You, X. Chen, Y. Zhang, C. Li, S. Li, Z. Liu, Z. Wang, and Y. Lin, “Shiftaddnet: A hardware-inspired deep network,” *ArXiv*, vol. abs/2010.12785, 2020.
- [9] H. Shi, H. You, Z. Wang, and Y. Lin, “Nasa $\$+\$$: Neural architecture search and acceleration for multiplication-reduced hybrid networks,” *IEEE Transactions on Circuits and Systems I: Regular Papers*, 2023.
- [10] H. Shi *et al.*, “Nasa-f: Fpga-oriented search and acceleration for multiplication-reduced hybrid networks,” *IEEE Transactions on Circuits and Systems I: Regular Papers*, pp. 1–14, 2023.
- [11] J. Yu *et al.*, “Bignas: Scaling up neural architecture search with big single-stage models,” in *European Conference on Computer Vision*, 2020.
- [12] D. Wang, C. Gong, M. Li, Q. Liu, and V. Chandra, “Alphanet: Improved training of supernet with alpha-divergence,” in *International Conference on Machine Learning*, 2021.
- [13] H. Wang, C. Ge, H. Chen, and X. Sun, “Prenas: Preferred one-shot learning towards efficient neural architecture search,” *arXiv preprint arXiv:2304.14636*, 2023.
- [14] H. Shi, H. You, Y. Zhao, Z. Wang, and Y. Lin, “Nasa: Neural architecture search and acceleration for hardware inspired hybrid networks,” *IEEE/ACM International Conference on Computer-Aided Design (ICCAD '22)*, 2022.
- [15] N. Lee, T. Ajanthan, and P. H. Torr, “Snip: Single-shot network pruning based on connection sensitivity,” *arXiv preprint arXiv:1810.02340*, 2018.
- [16] M. Lin, P. Wang, Z. Sun, H. Chen, X. Sun, Q. Qian, H. Li, and R. Jin, “Zen-nas: A zero-shot nas for high-performance image recognition,” in *Proceedings of the IEEE/CVF International Conference on Computer Vision*, 2021, pp. 347–356.
- [17] W. Chen, X. Gong, and Z. Wang, “Neural architecture search on imagenet in four gpu hours: A theoretically inspired perspective,” 2021.
- [18] C. Wang, G. Zhang, and R. Grosse, “Picking winning tickets before training by preserving gradient flow,” 2020.
- [19] H. Tanaka, D. Kunin, D. L. K. Yamins, and S. Ganguli, “Pruning neural networks without any data by iteratively conserving synaptic flow,” 2020.
- [20] L. Liu, S. Zhang, Z. Kuang, A. Zhou, J.-H. Xue, X. Wang, Y. Chen, W. Yang, Q. Liao, and W. Zhang, “Group fisher pruning for practical network compression,” 2021.
- [21] M. S. Abdelfattah, A. Mehrotra, Łukasz Dudziak, and N. D. Lane, “Zero-cost proxies for lightweight nas,” 2021.
- [22] H. Cai, C. Gan, and S. Han, “Once for all: Train one network and specialize it for efficient deployment,” *ArXiv*, vol. abs/1908.09791, 2019.
- [23] Y. Lin, M. Yang, and S. Han, “Naas: Neural accelerator architecture search,” *2021 58th ACM/IEEE Design Automation Conference (DAC)*, pp. 1051–1056, 2021.
- [24] Y. Zhang, Y. Fu, W. Jiang, C. Li, H. You, M. Li, V. Chandra, and Y. Lin, “Dna: Differentiable network-accelerator co-search,” *arXiv preprint arXiv:2010.14778*, 2020.
- [25] C. Hong, Q. Huang, G. Dinh, and S. Shao, “DOSA: One-loop DSE for DNN accelerators using differentiable models,” in *Architecture and System Support for Transformer Models (ASSYST @ ISCA 2023)*, 2023. [Online]. Available: <https://openreview.net/forum?id=OHLhibN1Cr>
- [26] J. Zhang, J. Zhang, D. Huo, and H. Chen, “Anas: Asynchronous neuromorphic hardware architecture search based on a system-level simulator,” in *2023 60th ACM/IEEE Design Automation Conference (DAC)*, 2023, pp. 1–6.
- [27] Z. Liu, G. Li, and J. Cheng, “Efficient accelerator/network co-search with circular greedy reinforcement learning,” *IEEE Transactions on Circuits and Systems II: Express Briefs*, vol. 70, no. 7, pp. 2615–2619, 2023.
- [28] M. Dong, X. Chen, Y. Wang, and C. Xu, “Improving lightweight addernet via distillation from l2 to l1-norm,” *IEEE Transactions on Image Processing*, 2023.
- [29] H. You, B. Li, H. Shi, Y. Fu, and Y. Lin, “Shiftaddnas: Hardware-inspired search for more accurate and efficient neural networks,” in *International Conference on Machine Learning*, 2022. [Online]. Available: <https://api.semanticscholar.org/CorpusID:248834483>
- [30] H. You, H. Shi, Y. Guo, Yingyan, and Lin, “Shiftaddvit: Mixture of multiplication primitives towards efficient vision transformer,” 2023.
- [31] B. Wu *et al.*, “Fbnet: Hardware-aware efficient convnet design via differentiable neural architecture search,” *2019 IEEE/CVF Conference on Computer Vision and Pattern Recognition (CVPR)*, pp. 10726–10734, 2019.
- [32] A. Wan *et al.*, “Fbnetv2: Differentiable neural architecture search for spatial and channel dimensions,” *2020 IEEE/CVF Conference on Computer Vision and Pattern Recognition (CVPR)*, pp. 12962–12971, 2020.
- [33] X. Dai *et al.*, “Fbnetv3: Joint architecture-recipe search using predictor pretraining,” *2021 IEEE/CVF Conference on Computer Vision and Pattern Recognition (CVPR)*, pp. 16271–16280, 2021.
- [34] G. Li, S. K. Mandal, U. Y. Ogras, and R. Marculescu, “Flash: Fast neural architecture search with hardware optimization,” 2021.
- [35] Y. Zhang, Y. Fu, W. Jiang, C. Li, H. You, M. Li, V. Chandra, and Y. Lin, “Dna: Differentiable network-accelerator co-search,” 2020.
- [36] A. G. Howard, M. Sandler, G. Chu, L.-C. Chen, B. Chen, M. Tan, W. Wang, Y. Zhu, R. Pang, V. Vasudevan, Q. V. Le, and H. Adam, “Searching for mobilenetv3,” *2019 IEEE/CVF International Conference on Computer Vision (ICCV)*, pp. 1314–1324, 2019.
- [37] M. Sandler, A. Howard, M. Zhu, A. Zhmoginov, and L.-C. Chen, “Mobilenetv2: Inverted residuals and linear bottlenecks,” in *Proceedings of the IEEE conference on computer vision and pattern recognition*, 2018, pp. 4510–4520.
- [38] V. Lopes, S. Alirezazadeh, and L. A. Alexandre, *EPE-NAS: Efficient Performance Estimation Without Training for Neural Architecture Search*. Springer International Publishing, 2021, p. 552–563. [Online]. Available: http://dx.doi.org/10.1007/978-3-030-86383-8_44
- [39] M. G. Kendall, “A new measure of rank correlation,” *Biometrika*, vol. 30, no. 1/2, pp. 81–93, 1938.
- [40] H. Xiong, L. Huang, M. Yu, L. Liu, F. Zhu, and L. Shao, “On the number of linear regions of convolutional neural networks,” 2020.
- [41] Z. Sun *et al.*, “Zendet: Revisiting efficient object detection backbones from zero-shot neural architecture search,” 2021.
- [42] G. Li, D. Hoang, K. Bhardwaj, M. Lin, Z. Wang, and R. Marculescu, “Zero-shot neural architecture search: Challenges, solutions, and opportunities,” *arXiv preprint arXiv:2307.01998*, 2023.
- [43] K. Bhardwaj, J. Ward, C. Tung, D. Gope, L. Meng, I. Fedorov, A. Chalfin, P. Whatmough, and D. Loh, “Restructurable activation networks,” 2022.
- [44] J. Lee, Y. Bahri, R. Novak, S. S. Schoenholz, J. Pennington, and J. Sohl-Dickstein, “Deep neural networks as gaussian processes,” 2018.
- [45] E. Real *et al.*, “Regularized evolution for image classifier architecture search,” in *AAAI*, 2019.
- [46] Y.-H. Chen *et al.*, “Eyeriss: An energy-efficient reconfigurable accelerator for deep convolutional neural networks,” *IEEE Journal of Solid-State Circuits*, vol. 52, pp. 127–138, 2017.
- [47] Y. Shen, M. Ferdman, and P. Milder, “Maximizing cnn accelerator efficiency through resource partitioning,” in *2017 ACM/IEEE 44th Annual International Symposium on Computer Architecture (ISCA)*. IEEE, 2017, pp. 535–547.
- [48] Xilinx, “Wp486: Deep learning with int8 optimization on xilinx devices,” in *White Paper*, 2017.